AFRL-RX-WP-JA-2020-0320

ANALYSIS OF MULTI-STABLE ARCHITECTURES FOR MORPHING STRUCTURES (POSTPRINT)

Anil Erol and Jeffery Baur

AFRL/RXCC

5 May 2020
Interim Report

DISTRIBUTION STATEMENT A.
Approved for public release: distribution is unlimited.

© OPEN ACCESS

(STINFO COPY)

AIR FORCE RESEARCH LABORATORY
MATERIALS AND MANUFACTURING DIRECTORATE
WRIGHT-PATTERSON AIR FORCE BASE, OH 45433-7750
AIR FORCE MATERIEL COMMAND
UNITED STATES AIR FORCE

REPORT DOCUMENTATION PAGE

Form Approved
OMB No. 0704-0188

The public reporting burden for this collection of information is estimated to average 1 hour per response, including the time for reviewing instructions, searching existing data sources, gathering and maintaining the data needed, and completing and reviewing the collection of information. Send comments regarding this burden estimate or any other aspect of this collection of information, including suggestions for reducing this burden, to Department of Defense, Washington Headquarters Services, Directorate for Information Operations and Reports (0704-0188), 1215 Jefferson Davis Highway, Suite 1204, Arlington, VA 22202-4302. Respondents should be aware that notwithstanding any other provision of law, no person shall be subject to any penalty for failing to comply with a collection of information if it does not display a currently valid OMB control number. **PLEASE DO NOT RETURN YOUR FORM TO THE ABOVE ADDRESS**.

1. REPORT DATE *(DD-MM-YY)*	2. REPORT TYPE	3. DATES COVERED *(From - To)*
5 May 2020	Interim	22 July 2013 – 5 April 2020

4. TITLE AND SUBTITLE
Analysis of Multi-stable Architectures for Morphing Structures (Postprint)

5a. CONTRACT NUMBER
In House

5b. GRANT NUMBER

5c. PROGRAM ELEMENT NUMBER

6. AUTHOR(S)
Anil Erol and Jeffery Baur –
AFRL/RXCC
(Continued on next page)

5d. PROJECT NUMBER

5e. TASK NUMBER

5f. WORK UNIT NUMBER
X0S7

7. PERFORMING ORGANIZATION NAME(S) AND ADDRESS(ES)
AFRL/RX
2977 Hobson Way (Continued on next page)
Wright-Patterson AFB OH 45433

8. PERFORMING ORGANIZATION REPORT NUMBER

9. SPONSORING/MONITORING AGENCY NAME(S) AND ADDRESS(ES)
Air Force Research Laboratory
Materials and Manufacturing Directorate
Wright-Patterson Air Force Base, OH 45433-7750
Air Force Materiel Command
United States Air Force

10. SPONSORING/MONITORING AGENCY ACRONYM(S)
AFRL/RXCC

11. SPONSORING/MONITORING AGENCY REPORT NUMBER(S)
AFRL-RX-WP-JA-2020-0320

12. DISTRIBUTION/AVAILABILITY STATEMENT
DISTRIBUTION STATEMENT A. Approved for public release: distribution is unlimited.

13. SUPPLEMENTARY NOTES
PA Case Number: 88ABW-2020-1638; Clearance Date: 5 May 2020. This document contains color. Journal article published in ASME 2020 Conference on Smart Materials, Adaptive Structures and Intelligent Systems, online 4 Nov 2020. © Open Access. The U.S. Government is joint author of the work and has the right to use, modify, reproduce, release, perform, display, or disclose the work. The final publication is available at https://doi.org/10.1115/SMASIS2020-2395

14. ABSTRACT ***(Maximum 200 words)***
The field of multi-stable structures has been steadily growing due to a wide range of potential applications including energy harvesting, MEMS, and mechanical logic. This work focuses on utilizing elastic energy trapping and snap-through phenomena of bistable unit cells to design a latticed, hierarchical multi-stable cylinder that can articulate up to 30 degrees from its center axis. The employment of bistable elements is hypothesized to reduce the total strain energy required to articulate the cylinder, and yield faster responses with the snap-through. While multi-stable cylinders exist in previous studies, there have been no previous attempts at studying different modes of deformation beyond compressive loading. Thus, the current work presents a new problem regarding the effects of bistable elements in a latticed cylinder that is carrying tensile, compressive, and shear loadings and exhibiting large displacements as the cylinder is articulated. The total strain energy density of the articulating cylinder is investigated as a function of the heights of the unit cells, which aids in determining an ideal height for the design that minimizes the strain energy density. Results show that the strain energy of an articulating cylinder can be minimized with the use of multistability, and that a multi-stable cylinder can require up to three times less loads to maintain desired articulation compared to a mono-stable structure. In addition, the work in this study can yield methodologies for designing arbitrarily morphing skins beyond just cylindrical geometries.

15. SUBJECT TERMS
Morphing; bistable; multistable; articulation; nonlinear mechanics; buckling;

16. SECURITY CLASSIFICATION OF:			17. LIMITATION OF ABSTRACT:	18. NUMBER OF PAGES	19a. NAME OF RESPONSIBLE PERSON (Monitor)
a. REPORT	b. ABSTRACT	c. THIS PAGE			Hilmar Koerner
Unclassified	Unclassified	Unclassified	SAR	13	19b. TELEPHONE NUMBER *(Include Area Code)* (937) 255-9324

REPORT DOCUMENTATION PAGE Cont'd

6. AUTHOR(S)

Anil Erol and Jeffery Baur - AFRL/RXCC

7. PERFORMING ORGANIZATION NAME(S) AND ADDRESS(ES)

AFRL/RX
2977 Hobson Way
Wright-Patterson AFB OH 45433

Check for updates

Proceedings of the ASME 2020 Conference on Smart Materials, Adaptive Structures and Intelligent Systems
SMASIS2020
September 15, 2020, Virtual, Online

SMASIS2020-2395

Downloaded from http://asmedigitalcollection.asme.org/SMASIS/proceedings-pdf/SMASIS2020/84027/V001T04A025/6588160/v001t04a025-smasis2020-2395.pdf by Wrigh Research Site- AFRL user on 07 January 2021

ANALYSIS OF MULTI-STABLE ARCHITECTURES FOR MORPHING STRUCTURES

Anil Erol[1], Jeffery Baur[2]
Materials and Manufacturing Directorate
The Air Force Research Laboratory
Wright-Patterson, OH

ABSTRACT

The field of multi-stable structures has been steadily growing due to a wide range of potential applications including energy harvesting, MEMS, and mechanical logic. This work focuses on utilizing elastic energy trapping and snap-through phenomena of bistable unit cells to design a latticed, hierarchical multi-stable cylinder that can articulate up to 30 degrees from its center axis. The employment of bistable elements is hypothesized to reduce the total strain energy required to articulate the cylinder, and yield faster responses with the snap-through. While multi-stable cylinders exist in previous studies, there have been no previous attempts at studying different modes of deformation beyond compressive loading. Thus, the current work presents a new problem regarding the effects of bistable elements in a latticed cylinder that is carrying tensile, compressive, and shear loadings and exhibiting large displacements as the cylinder is articulated.. The total strain energy density of the articulating cylinder is investigated as a function of the heights of the unit cells, which aids in determining an ideal height for the design that minimizes the strain energy density. Results show that the strain energy of an articulating cylinder can be minimized with the use of multi-stability, and that a multi-stable cylinder can require up to three times less loads to maintain desired articulation compared to a mono-stable structure. These results will lead to future works on further optimizing the articulating cylinder by varying additional parameters like the individual heights of rows, the thicknesses of unit cell beams, the strain energy density, and the initial loading threshold for articulation. In addition, the work in this study can yield methodologies for designing arbitrarily morphing skins beyond just cylindrical geometries.

Keywords: Morphing, Bistable, Multistable, Articulation, Nonlinear Mechanics, Buckling.

INTRODUCTION

Bistability has been the focus of studies in recent years due to its wide range of applications in the aerospace, biomedicine, and energy industries. Structures or materials that can exist in two or more stable mechanical states are desirable for morphing [1] and energy harvesting [2-4]. Recent advances in additive manufacturing have even suggested that mechanical computers can be viable with the use of bistable micro-elements [5,6].

Mechanical bistability is the existence of two stable states of deformation in a material and structure. The stable configurations, or equilibria, can be visualized as the wells in an energy versus deformation plot (Figure 1). As the material transitions from one stable position to another, it must overcome a peak energy threshold, often referred to as a "snap-through." Bistability can be achieved via multiple mechanisms. The earliest known mechanism of bistability was reported in the early 1980's in unsymmetric laminates after curing [7]. These types of laminates experience bistability due to residual thermal stresses after curing. Some researchers have also achieved bistability in laminates by pre-stressing a layer during fabrication [8].

Other mechanisms for bistabiliy have since been discovered, including those based on buckling beams. While early beam-based bistable designs relied on hinged or pre-stressed beams, a monolithic structure fabricated with two pre-curved beams was proposed, as it did not rely on pre-stressing or multiple components [9]. Furthermore, due to advancements in 3D printing, fabricating structures based on the monolithic curved-beam design, referred to hereafter as "double curved beams," is much more feasible, especially on complex geometries. In fact,

[1] Contact author: anil.erol.ctr@us.af.mil
[2] Authors with shared affiliations should be placed together with their names separated by commas in the correct author order.

This material is declared a work of the U.S. Government and is not subject to copyright protection in the United States.
Approved for public release. Distribution is unlimited.

Distribution Statement A. Approved for public release (PA): distribution is unlimited.

researchers have already 3D printed lattices of these double curved beams to induce multi-stable behavior with higher order stability [10-12]. Additionally, others have 3D printed double-curved beam mechanisms on more complex geometries, such as cylinders, and studied the compressive behavior [13].

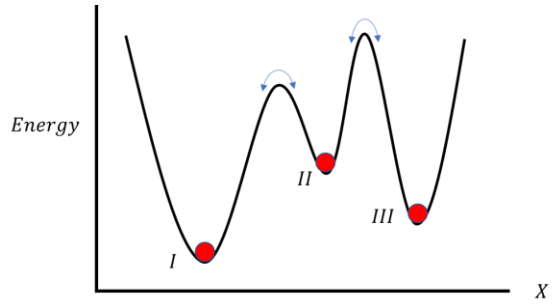

FIGURE 1. ENERGY OF A MATERIAL OR STRUCTURE AS A FUNCTION OF X, WHICH CAN BE ANY TYPE OF MECHANICAL DEFORMATION OR CONFIGURATION. THE MINIMA OR WELLS IN THE ENERGY ARE POSITIONS OF STABLE EQUILIBRIA. A MULTI-STABLE MATERIAL CAN HAVE TWO OR MORE STABLE STATES, SUCH AS THOSE DENOTED BY THE WELLS AT I, II, AND III ON THE CURVE. THE REGIMES BETWEEN THE STABLE POSITIONS CONTAIN ENERGY THRESHOLDS COMMONLY REFERRED TO AS "SNAP-THROUGH."

One area of application particularly attractive for multi-stability is morphing skins. Multi-stable structures are advantageous since they require less energy to deform into and maintain a non-initial shape, and they can bias a structure toward desired modes of deformation. Design concepts utilizing instability-based unit cells have been considered in the past two decades, but there has not been extensive applications of bistable unit cells due to difficulty in manufacturing and modeling structures [Thill, et al. 2008]. Recent advances in computing, finite element solvers, and 3D printing have opened a clear path toward designing and optimizing bistable or multi-stable morphing structures. One such structure is an articulating cylinder, which is of interest to the Air Force. However, besides being paramount to Air Force applied research, bending cylinders can be used in other applications, including industrial engineering (transportation and organization of products in warehouses for fabrication or delivery), A/C ventilation (tubes redistributing heat based on needs of system), and biomedicine (stents, catheters, and other minimally invasive material development). Furthermore, articulating cylinders can be viewed as a basic unit structure for the development of larger and more complex morphing structures. For instance, they can help build the framework for geometries such as 3-dimensional lattices useful in a wide range of morphing applications.

The goal of the current work is to make progress on developing methods for designing a "generalized" morphing skin. To achieve this goal, the double curved beam is selected as the basic unit cell for a multi-stable cylinder, as it requires a single type of material, and can achieve the type of deformation resulting in the articulation of the cylinder. The unit cell is studied via an optimization routine to determine the range of material properties viable for bistability. The goal of the optimization is to determine the efficacy of the chosen objective functions in terms of adequately measuring the "bistability" of the unit cell. Additionally, the results of the optimization will prove useful in a future optimization of the full-scale multi-stable cylinder. Namely, the relationships between geometric parameters (e.g. height and thickness of curved beam) and the objective functions measuring bistability are of particular interest for designing an optimized multi-stable cylinder.

The next part of the study introduces a design concept for an axi-symmetrically articulating cylinder. This design is a hybrid of two starting states of the unit cell, which enables the cylinder to articulate in any direction.

METHODS

Consider a hollow cylinder with a height H and thickness t_{cyl} defined by $t_{cyl} = R_o - R_i$, where R_o is the outer radius and R_i is the inner radius as defined in Figure 2. The cylinder occupies the space $\boldsymbol{B}$ with a boundary $\boldsymbol{\partial B}$, and it deforms via a mapping $\boldsymbol{\Theta}$ such that a point $\boldsymbol{x}$ in the deformed state can be determined by $\boldsymbol{x} = \boldsymbol{\Theta}(\boldsymbol{X}, \boldsymbol{P})$, where $\boldsymbol{X}$ is the corresponding material point in the initial state and $\{\boldsymbol{P}\}$ is a set of body loads and tractions. The articulation θ is defined by $\hat{\boldsymbol{n}} \cdot \hat{\boldsymbol{e}}_3 = cos\theta$, where $\hat{\boldsymbol{n}}$ is a vector normal to $\boldsymbol{\partial B}$ (initially $\hat{\boldsymbol{n}} = \hat{\boldsymbol{N}}$ as shown in Figure 2), and $\hat{\boldsymbol{e}}_3$ is part of the basis $\{\hat{\boldsymbol{e}}_1, \hat{\boldsymbol{e}}_2, \hat{\boldsymbol{e}}_3\}$ spanning 3-dimensional Euclidean space. The deformation of the body at this point is kept arbitrary, as it could depend on the type of bistable mechanism.

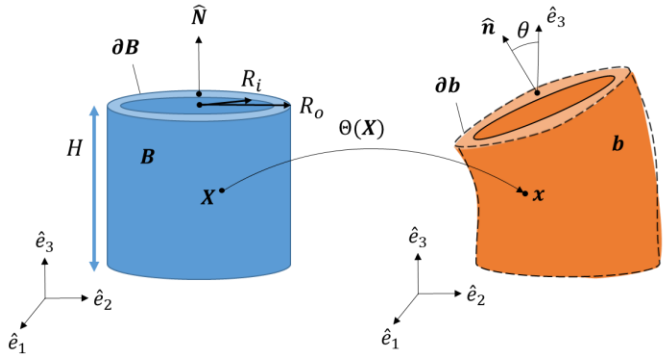

FIGURE 2. THE ARTICULATION OF THE CYLINDER, DENOTED BY BODY $\boldsymbol{B}$, IS DEPICTED IN ITS INITIAL AND DEFORMED CONFIGURATIONS. THE CYLINDER IS DEFINED BY GEOMETRIC DIMENSIONS R_i, R_o AND H REPRESENTING THE INNER RADIUS, OUTER RADIUS, AND HEIGHT OF THE CYLINDER, RESPECTIVELY.

2.1 Bistable Unit Mechanism

The chosen mechanism for bistability is the double curved-beam unit cell, as shown in Figure 3. The shape function for the beam is given by

$$w_0 = \frac{h}{2}(W_1 + a_3 W_3), \qquad (1)$$

Downloaded from http://asmedigitalcollection.asme.org/SMASIS/proceedings-pdf/SMASIS2020/84027/V001T04A025/6588160/v001t04a025-smasis2020-2395.pdf by Wrigh Research Site- AFRL user on 07 January 2021

Distribution Statement A. Approved for public release (PA): distribution is unlimited.

where W_1 is the first buckling mode, $W_1(x) = 1 - \cos(2\pi x/l)$, and $W_3(x) = 1 - \cos(4\pi x/l)$ is a mode shape imperfection with coefficient parameter a_3 scaling the thickness of the beam as shown in Figure 3.

This unit cell will serve as the basis for a lattice covering the body of the cylinder. Its primary dimensions are the height, horizontal length, and thickness of the beam, which are h, l, and t, respectively. These geometric quantities determine the response of the bistable unit cell since the beam element is the only region of the unit cell that deforms. The heights of blocks A and B, which are H_A and H_B, and the widths of the blocks, W_A and W_B, are secondary parameters are not directly related to the response of the bistable unit cell. Instead, they are either dependent on the primary parameters or can be manipulated to efficiently pack the unit cells across the body. For example, $H_A \geq h$ must be satisfied if the beam is expected to fully buckle down, and W_A can be used to properly pack a whole number of unit cells around the circumference of the cylinder.

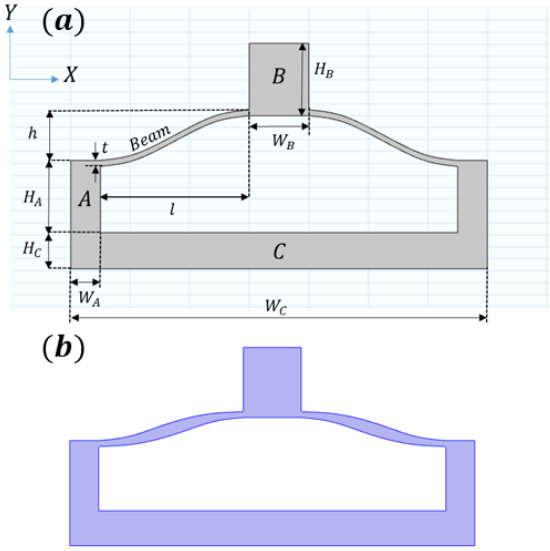

FIGURE 3. SCHEMATIC OF A BISTABLE UNIT CELL CONSISTING OF THREE TYPES OF BLOCKS, A, B, C, AND A CURVED BEAM IS SHOWN IN (a). THE UNIT CELL IS SYMMETRIC ABOUT THE Y-AXIS. THE MODE SHAPE IMPERFECTION WITH $a_3 \neq 0$ IN THE BEAMS IS SHOWN IN (b).

The double curved beam unit cell can be modeled both analytically and numerically. Analytical methods have been developed for it, utilizing the buckling mechanics of a beam constrained to planar motion [Qiu, 2004]. This method reduces a bistable unit cell to only its ligaments, which experience most of the deformation, and models the buckling of the ligament with beam theory, assuming the shape modes throughout deformation. The method has been expanded for unit cells on a cylindrical surface, where additional tractions due to the curvature of the cylinder are introduced [Hua, et al. 2019]. While these methods can produce quick and insightful results, they are limited to a single degree of freedom (i.e. a 1D vertical movement in the Y-direction). However, double curved beam unit cells on a cylinder that is articulating would experience multiple types of deformation. For example, some of the unit cells would experience shear, forcing the center point block B (Figure 3) to also move in the X-direction. Thus, an analytical model would need to be developed for a bistable unit cell that has at least two degrees of freedom (possibly more, if block B is allowed to rotate as it would on the side of an articulating cylinder). Since the analytical models for a single DOF buckling unit cell already require convoluted derivations and solution methods, the current work will utilize finite element methods for optimization, leaving the development of a higher-order analytical model for future works.

2.2 FINITE ELEMENT MODEL

The finite element model is developed in COMSOL using a 2D plane strain approximation with the same dimensions shown in Figure 3 parametrized. The continuum-based solid mechanics module is employed. The governing equations are represented by the equilibrium,

$$0 = \nabla \cdot (\boldsymbol{F}\boldsymbol{S})^T + \boldsymbol{P}v \tag{2}$$

where $\boldsymbol{F}$ is the deformation gradient, $\boldsymbol{S}$ is the second Piola-Kirchoff stress tensor, $\boldsymbol{P}$ is body loads, $\nabla\cdot$ is the standard divergence operation, and v is the density of the material. The stress tensor $\boldsymbol{S}$ is related to the strain $\boldsymbol{\varepsilon}$ by

$$\boldsymbol{S} = \frac{\partial W_s}{\partial \boldsymbol{\varepsilon}}, \tag{3}$$

where W_s is the elastic energy density. The strain $\boldsymbol{\varepsilon}$ is in the form of

$$\boldsymbol{\varepsilon} = \frac{1}{2}(F^T F - \boldsymbol{I}), \tag{4}$$

in which $\boldsymbol{I}$ is the identity tensor.

A nearly incompressible material model based on the Neo-Hookean hyperelastic model is chosen, in the form of

$$W_s = \frac{1}{2}\mu(\bar{I}_1 - 3) + \frac{1}{50}\kappa(J^5 + J^{-5} - 2), \tag{5}$$

where μ is the shear modulus, κ is the bulk modulus, $\bar{I}_1 = tr(\boldsymbol{\varepsilon})$ is the first strain invariant, and $J = \det(\boldsymbol{F})$ is the Jacobian [14].

The top edge (1 on Figure X) is prescribed a displacement in the negative y-direction by an amount H, and the bottom edge (2 on Figure X) is constrained. The remaining edges are left free to displace. To obtain a converged solution, the model is solved iteratively over a range of δ_y such that the previous solution is used to calculate the solution for the next δ_y, i.e., $\delta_{y,i} = \delta_{y,i-1} + \delta_{step}$. The step size δ_{step} is determined based on 30 steps in total for a moderately high resolution without significantly impairing computational time.

2.3 OPTIMIZATION OF UNIT CELL

Downloaded from http://asmedigitalcollection.asme.org/SMASIS/proceedings-pdf/SMASIS2020/84027/V001T04A025/6588160/v001t04a025-smasis2020-2395.pdf by Wrigh Research Site- AFRL user on 07 January 2021

Distribution Statement A. Approved for public release (PA): distribution is unlimited.

Since optimizing an entire multi-stable cylinder may be computationally cumbersome, a unit cell optimization problem is proposed. The goal of this method is to relate the local kinematics of the unit cells to the global kinematics of the cylinder to obtain an approximate solution to the bending of the cylinder. For the purpose of this preliminary study, one double curved beam unit cell under compression is treated as the representative element. This unit cell is prescribed a displacement $\partial_y{}'$ relating the local deformation of the unit cell to the global kinematics of a multi-stable cylinder with six rows of unit cells in the direction of the height, and eight columns of unit cells around the circumference. Assuming plane sections remain plane while the cylinder deforms, $\partial_y{}'$ can be determined by considering the length of a line on the compressive side (Figure 4) initially with length $L_C = H$. When the cylinder is articulated, its deformed length l_C is given by

$$l_C = \rho_C \theta, \tag{6}$$

where ρ_C is the radius coordinate ρ as defined in Figure 6 at point C. On the compressed outer surface, the value of ρ_C can be determined by the relation

$$\rho_C = \rho_N - R_o. \tag{7}$$

Since ρ_N coincides with the neutral axis of the cylinder, it is given by

$$\rho_N = \frac{H}{\theta}, \tag{8}$$

the substitution of (7) and (8) into (6) yields l_C in the form of

$$l_C = H - R_o \theta. \tag{9}$$

Next, the lengths of the unit cell in compression and tension can be determined by the dimensions provided in Figure 3, such that a unit cell starting in initial position 1 has a height h_1 given by

$$h_1 = H_A + H_B + H_C + h - t, \tag{10}$$

and a unit cell starting in a buckled position 2 has a height h_2 of

$$h_1 = H_A + H_B + H_C - h - t, \tag{11}$$

Thus, with six rows of unit cells on the cylinder, three starting in position 1 and three starting in position 2, the total height of the cylinder $H = 3(h_1 + h_2)$ is given by

$$H = 6(H_A + H_B + H_C - t). \tag{12}$$

Note that due to the opposing signs of h in equations (10) and (11), the height term h vanishes when calculating for the expression for H.

To determine the amount of effective change in length $\Delta L_{c,eff}$ experienced on the compressive side of the hybrid cylinder, the following relation is introduced,

$$\Delta L_{c,eff} = H - l_C, \tag{13}$$

With the substitution of (9) into (13) for l_C, the expression for $\Delta L_{c,eff}$ can be written as

$$\Delta L_{c,eff} = R_o \theta. \tag{14}$$

Since only three rows of unit cells can snap-through under compression during articulation, the change in length is assumed to be evenly distributed among three unit cells such that $\partial_y{}' = \Delta L_{c,eff}/3$, which can be written as

$$\partial_y{}' = \frac{R_o \theta}{3}. \tag{19}$$

The current geometric derivation assumes that ideally, the snap-through of unit cells on all six rows will compensate for the shortening of l_C such that unit cells already buckled will not be deforming any further and block B of any unit cell will not hit block C.

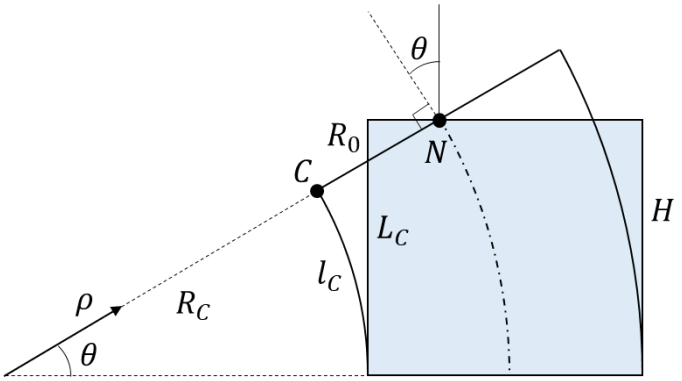

FIGURE 4. ASSUMED KINEMATIC RELATIONSHIPS OF THE ARTICULATION CYLINDER. IN THIS CASE, THE CYLINDER IS ASSUMED TO HAVE AN OUTER RADIUS R_o EQUIVALENT TO HALF ITS HEIGHT *H*.

The goal in this section is to formulate hypotheses for three objective functions for the optimization regarding how well they can measure aspects of bistability in the unit cell. The objective functions will depend on the results of the finite element simulation, which can measure strain energy density, reaction forces, and strains versus the prescribed displacement.

One of the primary reasons for implementing a bistable material in a morphing application is that an equilibrium in a target deformed position will mean that no load will be required to maintain that position, assuming deformation occurs in the linear elastic regime of the material. Thus, the goal is to align the second stable position with the target deformed state. A reaction force in the y-direction $R_y > 0$ implies that the snap-through has not occurred or the unit cell is being pushed past its second stable

Downloaded from http://asmedigitalcollection.asme.org/SMASIS/proceedings-pdf/SMASIS2020/84027/V001T04A025/6588160/v001t04a025-smasis2020-2395.pdf by Wrigh Research Site- AFRL user on 07 January 2021

Distribution Statement A. Approved for public release (PA): distribution is unlimited.

equilibrium (after snap-through). A reaction force $R_y < 0$ implies a deformed position between snap-through and second stable position. It is only when $R_y = 0$ that stability is maintained. Thus, one measure of stability must be the minimization of R_y. This yields the first hypothesis, which is that minimizing the reaction force at a prescribed displacement will sufficiently measure the stability at that deformed position. The first objective function can be written as

$$F_1 = abs\left(\frac{\mu I_z h}{l^3} R_y(\delta_{y,max})\right) \tag{15}$$

in which $abs(\cdot)$ is the absolute value function, and the coefficient is a non-dimensionalizing factor containing I_z, the moment of inertia of the cross-section of the beam about the z-axis. The reaction force in the Y-direction, R_y, is a function of the prescribed displacement, and in (15) it is taken at the maximum displacement.

The second advantage of bistability is a lower amount of strain energy needed to deform the material into the desired shape. Higher strain energy density at the deformed position means that more energy must be put into the system to achieve the deformation. Thus, the second hypothesis is that minimizing the strain energy density at the prescribed location will aid in yielding optimal bistable designs that require less energy than mono-stable counterparts. The second objective function can be written as

$$F_2 = W_t(\delta_{y,max}) \tag{16}$$

The third objective function will focus on the materials selection by considering the principal strains. Thus, the third hypothesis is that optimizing with respect to the maximum strain throughout the deformation will yield a material space for bistable morphing structures. The third objective function can be written as the measurement of the maximum strain observed in the structure,

$$F_3 = \max(\varepsilon'_{1,max}), \tag{17}$$

where ε'_1 is the first principal strain and $\varepsilon'_{1,max}$ is the maximum value across all material points at a given δ_y, and the outer maximum is applied on a set $\{\varepsilon'_{1,max}\}$ across all δ_y in set

$$\boldsymbol{\delta_y} = \{0, \delta_{step}, 2 * \delta_{step}, , \dots, \delta_{y,max}\}. \tag{18}$$

These three objective functions must be minimized by varying a set of geometric parameters directly influencing the bistable behavior of the unit cell. Three geometric parameters fit this criterion: h, l and t. This set can be reduced to two parameters by non-dimensionalization, $h^* = h/l$ and $t^* = t/l$

In addition, a third parameter a_3 modifying the shape of the beam is selected. Thus, the set of parameters is $\{h^*, t^*, a_3\}$. The optimization problem can be written as follows:

Find $\{h^*, t^*, a_3\}$ such that F_1, F_2, F_3 are minimized.

Subject to

$$0 = \nabla \cdot (\boldsymbol{FS})^T + \boldsymbol{F}v,$$
$$\boldsymbol{S} = \frac{\partial W_s}{\partial \varepsilon},$$
$$W_s = \frac{1}{2}\mu(\bar{I}_1 - 3) + \frac{1}{50}\kappa(J^5 + J^{-5} - 2),$$
$$h^*_{min} \le h^* \le h^*_{max},$$
$$a_{3min} \le a_3 \le a_{3max},$$
$$t^*_{min} \le t^* \le t^*_{max}.$$

2.4 INTRODUCTING A HYBRID CYLINDER DESIGN

In this section, a latticed cylinder based on the double curved beam is studied. This type of cylinder design already exists in literature, serving as a good starting point [13]. The existing design contains a lattice of unit cells all starting in the same initial position. Thus, if this cylinder design is articulated in any direction, only the unit cells on the compressive side will buckle into the second stable position. To address this issue, a hybrid structure is proposed, which consists of two types of rows: those starting in initial position 1, and those starting in buckled position 2 (see Figure 5.a). The hybrid design can thus take advantage of both the compressive and tensile sides, as shown in Figure 5.b and Figure 5.c.

The top surface is subjected to a prescribed rotation, and the bottom surface is constrained. To reduce computational time, the cylinder is cut in half and symmetric conditions are applied to the cut surfaces.

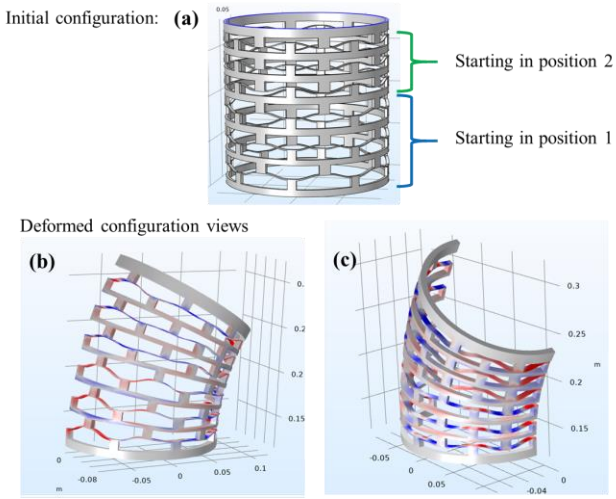

FIGURE 5. THE HYBRID DESIGN IS SHOWN IN (a) WITH TWO TYPES OF ROWS CONTAINING UNIT CELLS STARTING IN TWO DIFFERENT POSITIONS. THE DEFORMED SHAPES IN (b) AND (c) ARE ILLUSTRATIONS OF HOW THE ROWS WILL SNAP-THROUGH. THE TOP ROWS STARTING IN POSITION 2 WILL BUCKLE UP ON THE TENSILE SIDE IN (b) AND THE BOTTOM ROWS STARTING IN POSITION 1 WILL BUCKLE DOWN ON THE COMPRESSIVE SIDE IN (c). IN

Downloaded from http://asmedigitalcollection.asme.org/SMASIS/proceedings-pdf/SMASIS2020/84027/V001T04A025/6588160/v001t04a025-smasis2020-2395.pdf by Wrigh Research Site- AFRL user on 07 January 2021

Distribution Statement A. Approved for public release (PA): distribution is unlimited.

THIS MANNER, THE CYLINDER CAN ARTICULATE IN ANY DIRECTION WHILE UTILIZING SNAP-THROUGH ON BOTH SIDES.

RESULTS

The double curved beam unit cell was simulated with different values of bulk modulus κ to determine a feasible range of material properties and understand the effects of material properties on bistable behavior. For instance, the bistability of the unit cell depends on how much compressive strain energy is transferred into the bending strain energy as the beams buckle. Thus, an incompressible material will exhibit bistable behavior while a highly compressive material will not, particularly for beams with mode shape imperfections. Most materials fall somewhere between these extremes, and it is worthwhile to find the cutoff point between the two types of behavior, and analyze the effects of κ within each regime. The property of interest is the bulk modulus, κ, which is non-dimensionalized by $\kappa^* = \kappa/\mu$ (μ being the shear modulus), while the reaction force R_y on the unit cell is non-dimensionalized by

$$R_y{}^* = \frac{\mu I_z h}{l^3} R_y, \tag{19}$$

where I_z is the moment of inertia of the cross-section of the beam about the z-axis. The top surface of the unit cell is prescribed a displacement of $\partial_y = 2h$, and it is normalized by $\partial_y{}^* = \frac{\partial_y}{2h}$.

Figure 6 plots the results of eight simulations at different values of κ^*. Figure 6.a plots $R_y{}^*$ versus κ^* for a beam with no mode shape imperfections (i.e., the beams have the same cross section throughout their length). This type of beam has bistability throughout the range of κ^* the unit cell was simulated. The main trend in Figure 6.a is that an increasing κ^* increases the slope of the curves, indicating a higher force threshold for snap-through. This effect can be explained by the inability of incompressible beams to deform via compression, requiring higher shape modes to achieve snap-through. By contrtast, the plots for a unit cell with mode shape imperfections (Figure 6.b) exhibit both mono-stable and bistable behavior depending on κ^*. A highly compressible material with a bulk modulus of $\kappa^* = 10^{-4}$ shows no bistability, since the curve is monotonic with an almost linear slope. However, as κ^* increases, the curve becomes non-monotonic, such as at $\kappa^* = 0.01$, and at a high enough κ^*, the unit cell achieves a snap-through effect at approximately $\partial_y{}^* = 0.6$, and a second stable position at $\partial_y{}^* = 1$. The cutoff for bistable behavior is between $\kappa^* = 0.01$ and $\kappa^* = 0.1$.

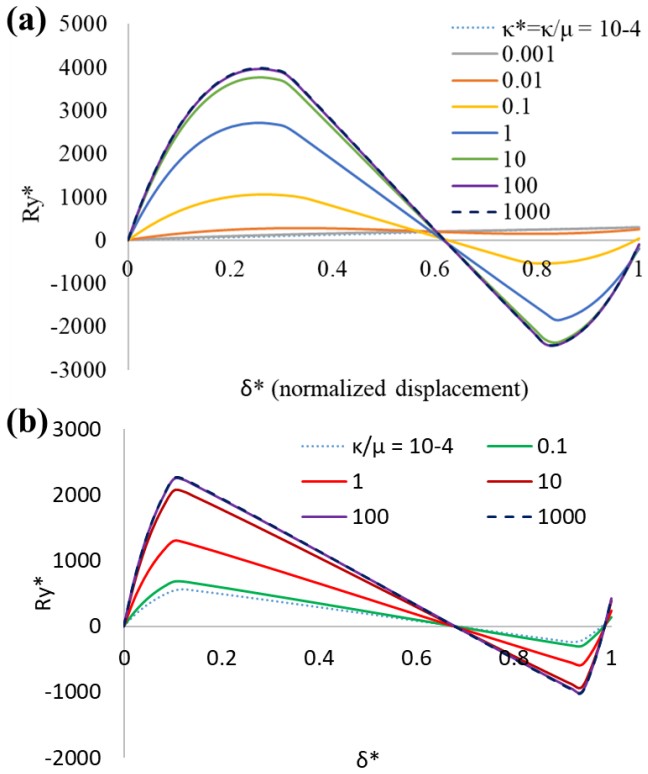

FIGURE 6. THE NON-DIMENSIONALIZED FORCE $R_y{}^*$ IS PLOTTED VERSUS NORMALIZED DISPLACEMENT $\partial_y{}^*$ FOR (a) WHEN $a_3 = 0$ AND (b) $a_3 = 0.3$. CHANGING THE BULK MODULUS RELATIVE TO THE SHEAR MODULUS FOR A NEO-HOOKEAN MATERIAL MODEL SHOWS THAT THERE IS A MINIMUM RATIO OF κ to μ WHEN THERE IS A MODE SHAPE IMPERFECTION.

3.1 OPTIMIZATION OF THE UNIT CELL

The unit cell optimization was performed via the modified NSGA-II genetic algorithm supported by MATLAB with a population size of 40 and with the remaining constants provided in Table 1.

TABLE 1. THE CONSTANTS USED FOR THE GENETIC ALGORITHM.

Parameter	Value
$h^*{}_{max}$	1.25
$h^*{}_{min}$	0
$a_{3_{max}}$	0.3
$a_{3_{min}}$	0
$t^*{}_{max}$	0.15
$t^*{}_{min}$	0.1
θ	$\pi/6$
R_o	0.177 m

The Pareto front is plotted in Figure 7 for the three objective functions. The designs on the Pareto front are individuals whose

Downloaded from http://asmedigitalcollection.asme.org/SMASIS/proceedings-pdf/SMASIS2020/84027/V001T04A025/6588160/v001t04a025-smasis2020-2395.pdf by Wrigh Research Site- AFRL user on 07 January 2021

Distribution Statement A. Approved for public release (PA): distribution is unlimited.

performances in any objective function cannot be increased by changing their parameters without decreasing their performance in another objective function. Designs 1, 2 and 3 are the individuals best performing in objective functions 1, 2, and 3, respectively. Their genes are listed in Table 2, along with their performances in each objective. There are some notable differences and similarities between the selected optimal designs. For instance, while there is significant variation in the performances in all three objectives, F_1 shows the greatest variation. Design 1 almost has zero reaction force compared to the other designs, indicating it is almost in perfect equilibrium at the prescribed displacement.

TABLE 2. THE GENES AND PERFORMANCES OF THE FOUR DESIGNS ANNOTATED IN FIGURE 7.

	1	2	3	4
h^*	1.13	1.10	1.07	1.11
a_3	0.0058	0.0011	0.0017	0.0045
t^*	0.10	0.10	0.10	0.10
F_1	0.9	790	2390	261
F_2	0.184	0.161	0.170	0.165
F_3	0.12	0.089	0.085	0.090

The trade-off between strain energy and maintaining force may not be obvious. At a first glance, the two objectives seem to have similar aims in determining how well stability is achieved in the system. In the case of the maintaining force, F_1, reaching zero means achieving exact equilibrium, whereas for strain energy density, a local minimum indicates equilibrium. However, in the case of the strain energy density, F_2, a zero energy state may not necessarily be observed in equilibrium. In fact, we are only concerned with the slope and the second derivative of the curve. Thus, even if a position is in equilibrium, the system may still possess a non-zero energy state. Furthermore, as evident from the definition of the strain energy density, as it is an integral of the stress over strain, the amount of stress across the deformation will be proportional to the energy transferred into the elastic energy. Thus, one may expect to reach equilibrium through two paths, where one requires far greater strain energy than the other. The paths will depend on parameters such as the height of the beam but not necessarily other parameters, such as the beam's thickness. In Table 2, it appears that thickness is converging on the minimum value, $t^*_{min} = 0.1$, that the algorithm was constrained to. Similarly, the mode shape imperfection in all designs is almost zero, near the minimum constraint. In contrast, the height appears to have a wider range of values. Recall the displacement $\partial_y{}'$ from (19), which can be normalized by $\partial_y{}^* = \partial_y{}'/l$. When evaluated at the constants given in Table 2, $\partial_y{}^* = 2.2$ for all cases. Thus, it is no coincidence that the range of heights within the Pareto front are about half $\partial_y{}^*$. More specifically, the height of the beam is directly related to the kinematics of the beam such that buckling will yield a displacement twice the height plus the thickness of the beam.

Nonetheless, some designs do not have heights perfectly matching the prescribed displacement, and this is because the algorithm sought a trade-off between bistability, strain energy, and maximum strain. Since a higher height yields a higher force versus displacement slope (Figure 6), the rest of the designs aimed to lower the height to reduce strain energy and maximum strain (at the cost of bi-stability measured by F_1). For instance, Design 2 requires considerably greater force to maintain the prescribed displacement, but requires 12.5% less strain energy and a material with 33% lower allowable maximum strain to achieve the same deformation. Likewise, Design 3 requires even greater force to achieve the same deformation, but with the least amount of max strain. Design 4 is chosen based on its position between the first three designs, achieving the prescribed displacement with relatively good performances in all three objectives.

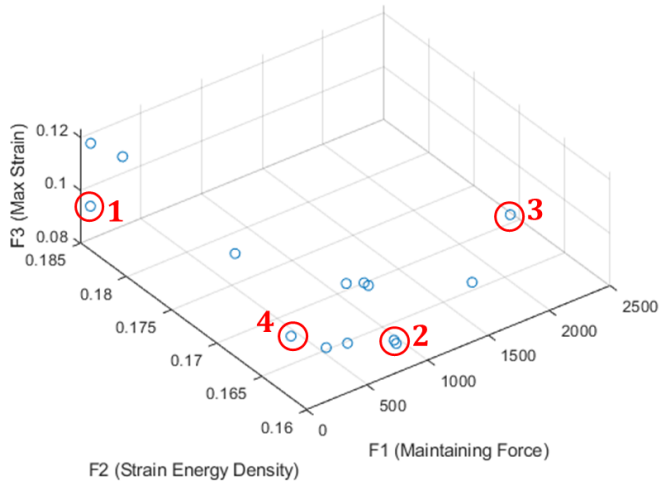

FIGURE 7. THE PARETO FRONT OBTAINED FROM THE GENETIC ALGORITHM OPTIMIZING THE UNIT CELL FOR THE THREE OBJECTIVE FUNCTIONS. DESIGNS 1, 2, AND 3 PERFORM BEST IN OBJECTIVE FUNCTIONS 1, 2, AND 3, RESPECTIVELY. DESIGN 4 IS AN EXAMPLE OF AN OPTIMAL DESIGN WITH A TRADE-OFF BETWEEN ALL THREE OBJECTIVES.

3.2 HYBRID CYLINDER SIMULATIONS

The hybrid cylinder was simulated up to 30 degrees of articulation at varying heights of the unit cells.

The simulations tested a few hypothoses, including (1) whether multi-stability can be achieved with local snap-through events, (2) if the amount of strain energy required to reach maximum articulation can be reduced with snap-through events and (3) if the amount of moment required to maintain articulation can be reduced with snap-through. A control case of $h^* = 0$ was also simulated for comparison. Figure 8.b provides examples of what the initial cylinder configurations look like at different values of h^*. The reaction moment is plotted versus articulation in Figure 8.a for ten values of h^* ranging from 0 to 1.29. At $h^* = 0$, the reaction moment monotonically increases versus articulation at a nonlinear rate, as expected from a mono-

Downloaded from http://asmedigitalcollection.asme.org/SMASIS/proceedings-pdf/SMASIS2020/84027/V001T04A025/6588160/v001t04a025-smasis2020-2395.pdf by Wrigh Research Site- AFRL user on 07 January 2021

Distribution Statement A. Approved for public release (PA): distribution is unlimited.

stable structure. As h^* increases, the slope of the curve gains a non-monotonic property as the effects of the bistable unit cells become more prominent. Furthermore, the curves exhibit non-monotonic behavior due to the buckling of the unit cells, effectively reducing the overall reaction moment required to maintain the articulation.

Multi-stability is defined as having two or more stable positions, and Figure 8.b contains two curves exhibiting this property. These curves are $h^* = 1$ (achieving stability at 5 and 9 degree articulation) and $h^* = 1.14$ (achieves stability at 5 and 16 degrees articulation). These points of stability occur at "dips" in the curve, the number of which directly correlates to the number of rows experiencing snap-through. Thus, to best utilize all six rows, the curve should have six dips (i.e. snap-throughs), with the location of the sixth dip achieving maximum articulation. The curve closest to achieving perfect alignment is $h^* = 1$, since it contains exactly six snap-through events with the sixth ending near 30 degrees articulation. At higher values of h^*, the heights of the rows are so large that not all rows have buckled at maximum articulation. Furthermore, larger h^*yields greater peaks in the curve, meaning that a larger load is required to achieve snap-through. Thus, Figure 8 illustrates another advantage of multi-stability in morphing structures: when multi-stability is properly leveraged (i.e., the stable positions align with desired target shape), a lower maximum load is required to morph the structure. The mono-stable curve requires almost three times as large of a moment to bend the cylinder to 30 degrees than the multi-stable curve at $h^* = 0.86$. This advantage can be essential in aerospace applications that cannot carry heavy mechanical systems to generate high loads.

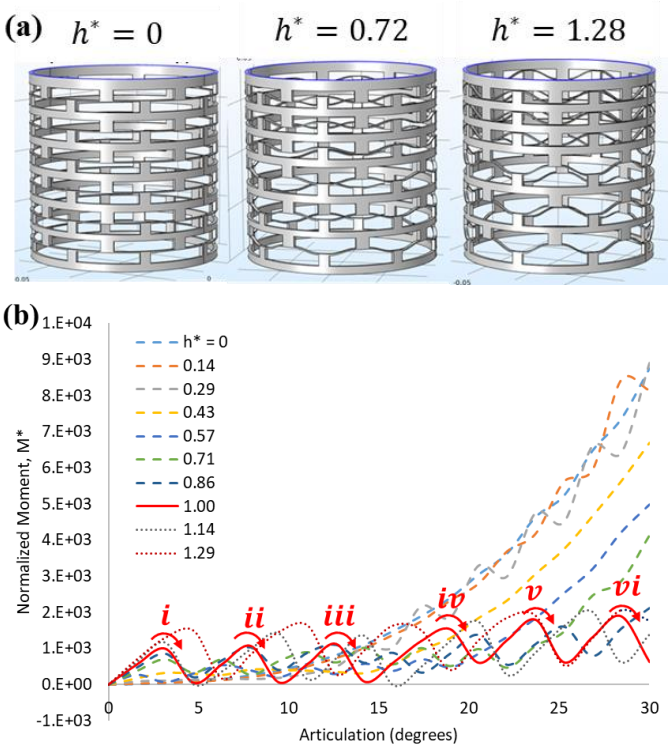

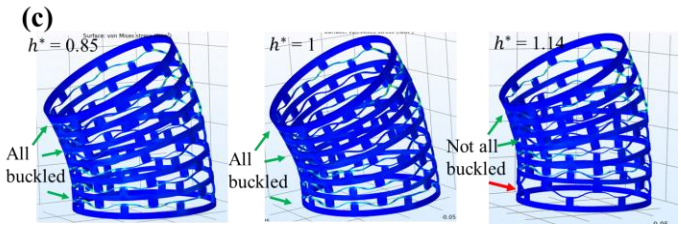

FIGURE 8. EXAMPLES OF THE CYLINDERS WITH DIFFERENT VALUES OF h^* FOR THE HEIGHT OF THE UNIT CELL ARE GIVEN IN (a), AND THE PLOTS OF THE REACTION MOMENT ON THE CYLINDER VERSUS THE RPESCRIBED ARTICULATION FOR VARIOUS h IS PROVIDED IN (b). SOME OF THE DEFORMED SHAPES AT MAXIMUM ARTICULATION ARE SHOWN IN (c).

The deformed shapes in Figure 8.c can also provide insights into the exact sequence of snap-through events among the six rows. The cylinder achieves snap-through in all rows for cylinders up to $h^* = 1$, which matches the curves in Figure 8.b. At $h^* = 1.14$, the bottom row of the articulated cylinder did not snap (Figure 8.c). These results also match those of the unit cell optimization, which found a range of h^* values between 1 and 1.2 on the Pareto front (Table 2), indicating that the local-to-global kinematics based entirely on the compressive side of an articulating cylinder can predict the approximate height of the unit cells needed for achieving efficient snap-through of all rows for a given degree of articulation.

The system can also be studied in terms of the strain energy density in the cylinder, which is plotted in Figure 9. The total strain-energy density would need to be minimized to take advantage of multi-stability in the cylinder. The minimum occurs at $h^* = 0.85$ based on the available data points, but a curve fit suggests that there may be a global minimum within the domain $[0.85,1)$. Interestingly, this minimum does not coincide with the curve closest to achieving the sixth snap-through at max articulation, which was around $h^* = 1$. This discrepancy is likely due to a trade-off between higher h^* requiring more strain energy for deformation, and the exact alignment of the snap-through's with the maximum articulation. Thus, while $h^* = 1$ has better alignment of snap-through's in all six rows with the same deformation, $h^* = 0.85$ requires a sufficiently lower moment to compensate for the additional deformation past the six snap-throughs required to achieve maximum articulation. Furthermore, it should be noted that the data set is incomplete, suggesting that there may be a global minimum elsewhere in the design space, which would best be determined by formal optimization.

Downloaded from http://asmedigitalcollection.asme.org/SMASIS/proceedings-pdf/SMASIS2020/84027/V001T04A025/6588160/v001t04a025-smasis2020-2395.pdf by Wrigh Research Site- AFRL user on 07 January 2021

Distribution Statement A. Approved for public release (PA): distribution is unlimited.

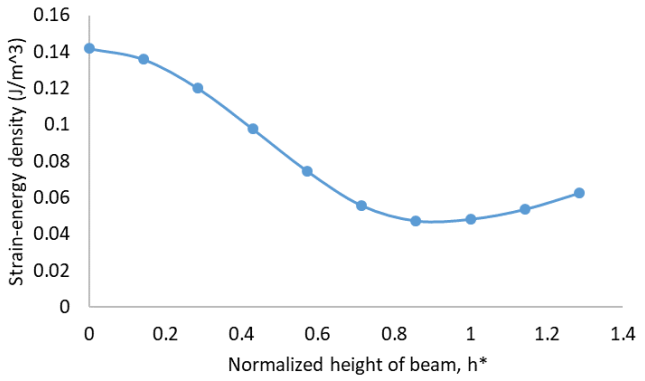

FIGURE 9. THE STRAIN ENERGY DENSITY IS PLOTTED VERSUS h^*.

CONCLUSIONS

In this study, bistable unit cells were used to construct a cylinder consisting of snap-through structures allowing it to articulate in any direction. A double curved beam mechanism was selected due to its monolithic material design and ease of implementation for a morphing structure. Simulations of the double curved beam unit cell showed a range of bistable behavior depending on a mode shape imperfection and the material's bulk modulus. If the beams do not have mode shape imperfections, then the bulk modulus only affects the magnitude of force required for snap-through. In contrast, with the mode shape imperfections, relatively compressible materials (i.e. low bulk modulus) cannot generate a bistable response.

The unit cell was also optimized *via* a genetic algorithm to determine how the height, thickness and mode shape imperfection of the beams influence bistable behavior. The optimization only simulated the unit cell, which served as an alternative method to simulating the entire cylinder with an array of bistable mechanisms. The goal of the unit cell optimization was to develop a method of utilizing a single unit cell to represent the overall structure by linking the local deformation to the global kinematics. The results in the Pareto front showed that optimal designs were found with minimized thicknesses and mode shape imperfections, suggesting that designers should aim to select the thinnest possible beams if their goal is to minimize strain energy density and applied loads. In addition, the optimal designs showed that the height of the beams must coincide with half the prescribed displacement (since the curved-beam buckles a distance that is twice its height), but the height can be adjusted in order to reduce the maximum allowable strain and energy input at the cost of losing bistability. However, it should be noted that the simulation was only performed on a 2D approximation of unit cells on the compressive side of a bending cylinder. Future works must address the type of loading on unit cells at other locations on the cylinder, such as those experiencing shear in non-1D buckling, as well as the proper boundary conditions.

Lastly, a hybrid design containing the unit cells on a cylinder was introduced to address the ability of the cylinder to take advantage of as many unit cells as possible when articulating in any direction. By constructing a cylinder with half the rows of unit cells starting in a buckled position, the cylinder was shown to achieve a multi-stable response for some unit cell geometries, and near-multi-stable properties for other geometries. Furthermore, the local bistable events significantly reduced the moment required to maintain the articulation by more than an order of magnitude compared to the standard mono-stable structure. A parametric sweep of the height of the unit cells showed that there may be an optimal height to minimize the strain energy density of the cylinder at the maximum articulation. Furthermore, the results of the cylinder simulations coincided with the results of the unit cell optimization in terms of finding the optimal height of the unit cells for buckling all rows. However, the cylinder simulations also revealed more complicated results, suggesting that the shear effects of unit cells may be influencing the behavior of the cylinder more significantly than previously thought. There is significant room for future work in developing and optimizing a full-cylinder model that allows for different unit cell heights at each row, which could drastically reduce the strain energy required to articulate the cylinder.

ACKNOWLEDGEMENTS

This research was performed while the author held an NRC Research Associateship award at the Air Force Research Laboratory.

REFERENCES

[1] Thill, C. L., et al. "Morphing skins." *The aeronautical journal* 112.1129 (2008): 117-139.

[2] Emam, Samir A., and Daniel J. Inman. "A review on bistable composite laminates for morphing and energy harvesting." *Applied Mechanics Reviews* 67.6 (2015).

[3] Pellegrini, Sergio P., et al. "Bistable vibration energy harvesters: a review." *Journal of Intelligent Material Systems and Structures* 24.11 (2013): 1303-1312.

[4] Zou, Hong-Xiang, et al. "Mechanical modulations for enhancing energy harvesting: Principles, methods and applications." *Applied Energy* 255 (2019): 113871.

[5] Song, Yuanping, et al. "Additively manufacturable micro-mechanical logic gates." *Nature communications* 10.1 (2019): 1-6.

[6] Sun, F., et al. *A study of Micro-Mechanical Logic Elements*. No. LLNL-PROC-781723. Lawrence Livermore National Lab.(LLNL), Livermore, CA (United States), 2019.

[7] Hyer, Michael W. "Some observations on the cured shape of thin unsymmetric laminates." *Journal of Composite Materials* 15.2 (1981): 175-194.

[8] Daynes, S., K. D. Potter, and P. M. Weaver. "Bistable prestressed buckled laminates." *Composites Science and Technology* 68.15-16 (2008): 3431-3437.

[9] Qiu, Jin, Jeffrey H. Lang, and Alexander H. Slocum. "A curved-beam bistable mechanism." *Journal of microelectromechanical systems* 13.2 (2004): 137-146.

Downloaded from http://asmedigitalcollection.asme.org/SMASIS/proceedings-pdf/SMASIS2020/84027/V001T04A025/6588160/v001t04a025-smasis2020-2395.pdf by Wrigh Research Site- AFRL user on 07 January 2021

Distribution Statement A. Approved for public release (PA): distribution is unlimited.

[10] Yang, Hang, and Li Ma. "Multi-stable mechanical metamaterials by elastic buckling instability." *Journal of materials science* 54.4 (2019): 3509-3526.
[11] Che, Kaikai, et al. "Three-dimensional-printed multistable mechanical metamaterials with a deterministic deformation sequence." *Journal of Applied Mechanics* 84.1 (2017).
[12] Rafsanjani, Ahmad, Abdolhamid Akbarzadeh, and Damiano Pasini. "Snapping mechanical metamaterials under tension." Advanced Materials 27.39 (2015): 5931-5935.
[13] Hua, Jian, et al. "Multistable Cylindrical Mechanical Metastructures: Theoretical and Experimental Studies." *Journal of Applied Mechanics* 86.7 (2019).
[14] Hartmann, Stefan, and Patrizio Neff. "Polyconvexity of generalized polynomial-type hyperelastic strain energy functions for near-incompressibility." International journal of solids and structures 40.11 (2003): 2767-2791.

Downloaded from http://asmedigitalcollection.asme.org/SMASIS/proceedings-pdf/SMASIS2020/84027/V001T04A025/6588160/v001t04a025-smasis2020-2395.pdf by Wrigh Research Site- AFRL user on 07 January 2021

Distribution Statement A. Approved for public release (PA): distribution is unlimited.